IEEE Robotics and Automation Letters (RAL) paper presented at the
2020 IEEE/RSJ International Conference on Intelligent Robots and Systems (IROS)
October 25-29, 2020, Las Vegas, NV, USA (Virtual)

Extremum Seeking Control for Stiffness Auto-Tuning of a Quasi-Passive Ankle Exoskeleton

Saurav Kumar[1,2], Matthew Richard Zwall[3], Edgar A. Bolívar-Nieto[3], Robert D. Gregg[4], and Nicholas Gans[5]

***Abstract*— Recently, it has been shown that light-weight, passive, ankle exoskeletons with spring-based energy store-and-release mechanisms can reduce the muscular effort of human walking. The stiffness of the spring in such a device must be properly tuned in order to minimize the muscular effort. However, this muscular effort changes for different locomotion conditions (e.g., walking speed), causing the optimal spring stiffness to vary as well. Existing passive exoskeletons have a fixed stiffness during operation, preventing it from responding to changes in walking conditions. Thus, there is a need of a device and auto-tuning algorithm that minimizes the muscular effort across different walking conditions, while preserving the advantages of passive exoskeletons. In this paper, we developed a quasi-passive ankle exoskeleton with a variable stiffness mechanism capable of self-tuning. As the relationship between the muscular effort and the optimal spring stiffness across different walking speeds is not known a priori, a model-free, discrete-time extremum seeking control (ESC) algorithm was implemented for real-time optimization of spring stiffness. Experiments with an able-bodied subject demonstrate that as the walking speed of the user changes, ESC automatically tunes the torsional stiffness about the ankle joint. The average RMS EMG readings of tibialis anterior and soleus muscles at slow walking speed decreased by 26.48% and 7.42%, respectively.**

I. INTRODUCTION

Recently, it has been shown that passive, light-weight ankle exoskeletons with a spring attached in parallel to the calf muscles can reduce the muscular effort of humans during walking [1]–[4]. However, the design of the components in such devices are optimized *offline* so as to produce the maximum reduction in muscular effort for a *particular* walking condition. As the walking conditions change (e.g., walking speed), the lower-limb muscular effort also changes [5]. Due to the use of passive components in these exoskeletons, assistive properties are fixed, and real-time adaptation to changing walking conditions is not possible. Thus, there is a need for a similar device that minimizes the muscular effort across different walking conditions, while preserving the advantages of passive exoskeletons.

Several passive ankle exoskeletons have been built in an attempt to reduce the muscular effort of human walking, such as [1]–[4]. In [1], [2], an elastic ankle exoskeleton with a spring connected in parallel to the calf muscle was shown to reduce the solueus muscle activity during hopping. Also, it was conjectured in [2] that the exoskeleton's spring stiffness needs to be tuned to achieve greater reductions in the muscular effort. This was confirmed in [3], [4] using a similar elastic ankle exoskeleton with a clutch mechanism, where experimental results demonstrated that for each walking speed there exists an optimal spring stiffness that produced the highest reduction in the muscular effort. However, these passive devices lack the ability to adapt in real-time to different walking conditions. In particular, the selection of an optimal spring in [3], [4] was found heuristically by manually testing various stiffness values in order to achieve the highest reduction in the muscular effort. Besides this procedure being time-consuming, it was also limited to a single walking speed. However, the muscular effort changes with walking speed, which would cause the optimal spring stiffness (torque assistance pattern) to vary as well [6].

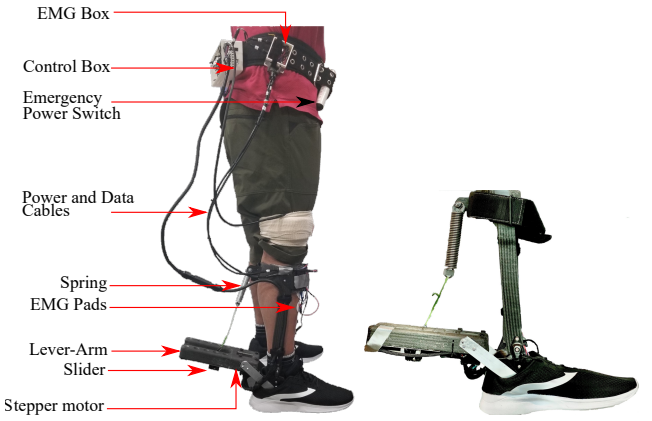

(a) Experimental setup (b) Quasi-passive exoskeleton

Fig. 1: (a) Experimental setup of a healthy subject wearing the quasi-passive ankle exoskeleton. The controllers and the batteries are mounted on the belt tied to the waist. (b) Actual manufactured version of ankle exoskeleton.

Apart from *offline* optimization of muscular effort with passive devices, efforts have been made in the field of active ankle exoskeletons to tune the joint parameters in real-time in order to improve the metabolic cost of the subject [6]–[8]. However, using the metabolic cost as an objective function leads to very slow adaptation that typically requires an hour to find a local optimum [9]. This slow process might not be applicable for adapting to real-time changes in behavior or environment. In addition, the measurement of the metabolic cost requires off-board sensors, e.g., face masks, which might be obtrusive to the user. Also, most of the active exoskeletons are restricted to the lab settings either due to the use of a heavy off-board motor [6], [10] or tethered air supply for

This work was supported by the National Science Foundation under Award Number 1728057 and 1830360 / 1953908. R. D. Gregg holds a Career Award at the Scientific Interface from the Burroughs Wellcome Fund.

[1]Department of Electrical Engineering, [2]Department of Bioengineering, [3]Department of Mechanical Engineering, The University of Texas at Dallas, Richardson, TX 75080, USA. [4]Department of Electrical and Computer Engineering, The University of Michigan, Ann Arbor, MI 48109, USA. [5]The University of Texas at Arlington Research Institute, University of Texas at Arlington, Arlington, TX 76019, USA. {sauravk,ebolivar,rgregg}@ieee.org, mrz130230@utdallas.edu, ngans@uta.edu

pneumatically actuated exoskeletons [8], [11]–[13].

Quasi-passive exoskeletons combine the adaptability of active exoskeletons with the autonomy of passive exoskeletons. In particular, these devices have passive components like springs [1], [2], dampers [14], [15] and also contains sensors, batteries and other electronics, but motors do not provide power directly to the human joint [16]. A quasi-passive leg exoskeleton consisting of variable-damping mechanism at the knee joint was presented in [14], [15]. In this paper, we developed a quasi-passive ankle exoskeleton that is able to adjust automatically through a range of torsional stiffness about the ankle joint via an adjustable lever-arm. Using this device, we conducted walking experiments at different walking speeds with the biological feedback provided by the electromyography (EMG) sensors (see Fig. 1a). Due to the unknown underlying dynamics and noisy EMG measurements, we used a model-free extremum seeking control (ESC) to perform real-time tuning of torsional stiffness of the exoskeleton in order to reduce the muscular effort of walking. The ESC uses a low-frequency perturbation signal to estimate the gradient of the cost function, making it more robust to noisy measurements [17]. Our experiments demonstrated that ESC was able to automatically tune the torsional stiffness of the ankle exoskeleton across different walking speeds. In particular, there are two important contributions of this paper.

Contributions of this paper

i) We built an unilateral quasi-passive ankle exoskeleton with a variable stiffness mechanism. To the best of our knowledge, this is the first quasi-passive device capable of real-time adaptation of stiffness in response to muscular activity at varying walking conditions.

ii) In order to perform real-time optimization of the muscular effort, we implemented a model-free control algorithm, ESC, to automatically tune the stiffness of the system across different walking speeds. The advantage of using an ESC is that it does not need the knowledge of the underlying dynamics. Walking experiments demonstrate a noticeable reduction in the muscular effort using our ESC algorithm. In addition, ESC adapts the stiffness of the system within 10 seconds as the walking speeds change.

The paper is organized as follows. In Section II, we describe the mechatronic design of the quasi-passive ankle exoskeleton and the discrete-time ESC algorithm for real-time stiffness tuning of the exoskeleton. In Section III, we describe the experimental setup and protocol followed for walking experiments. Next, we present the baseline and ESC experimental results in Section IV. We discuss these results and the limitations of this study in Section V. Finally, Section VI concludes the paper.

II. Design and Implementation

The quasi-passive ankle exoskeleton consists of a spring that stores energy during the early and mid-stance phase of walking and then releases it during push-off. The energy released by the spring during push-off provides assistive force to the plantar flexor muscles. In this section, we describe the design of our quasi-passive ankle exoskeleton and the variable stiffness lever, its embedded sensing capabilities, and the discrete-time perturbation-based ESC algorithm used to modify the torsional stiffness of the device.

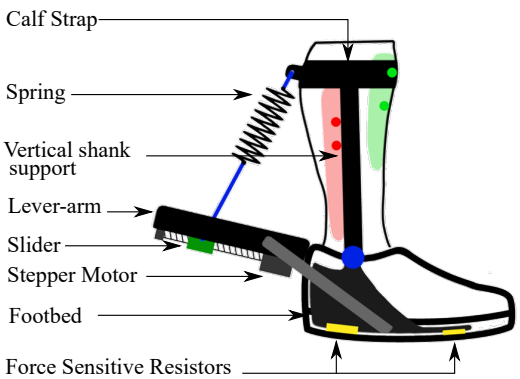

Fig. 2: Schematic of a quasi-passive ankle exoskeleton. The linear actuator comprising of the stepper motor and the slider mechanism is used to vary the torsional stiffness about the ankle joint. The shaded red and green areas show the approximate locations of the soleus and tibialis anterior muscles, respectively. The red and green dots indicate the approximate EMG placement locations.

A. Exoskeleton Design

We built a unilateral ankle exoskeleton with a variable stiffness mechanism, as shown in Fig. 1b. The exoskeleton has a carbon-fiber frame and a lever-arm assembly consisting of a slider and a stepper motor. The frame was made up of a vertical shank support and a footbed connected to the ankle joint. A free motion Tamarack Flexure Joint^{TM} was used at the ankle joint to reduce the weight of the device. This joint style was chosen to allow for minor inversion and eversion motion at the ankle joint to minimize the impact on the user's natural gait. Attached to the footbed section of the device is a lever-arm assembly with a variable attachment point for the spring. This point was connected by a cable to a coil spring anchored at the top of the frame near the calf muscle, as shown in Fig. 2. The position of the variable attachment point controls the system's torsional stiffness about the ankle joint (see Section II-B). The top of the vertical shank support is secured just below the user's knee with a padded Velcro strap, and the footbed was placed in an athletic shoe allowing it to be secured to the user's foot. A pair of force sensitive resistors (FSR) were placed on the foot sole for gait cycle detection, as shown in Fig. 2.

B. Variable Stiffness Lever Design

In order to vary the torsional stiffness about the ankle joint in our exoskeleton, we built a lever-arm to have a variable-effective length, as shown in Fig. 3. The lever-arm design consists of a MiSUMi^{TM} ball screw assembly mounted in a rigid frame. A slider attached to the ball nut includes an attachment point for the spring and bilateral wings to transfer force generated by the spring to the frame, preventing radial loading of the ball screw. The ball screw has a lead of 2 mm and is powered by a QMot QSH2818 Trinamic Motion

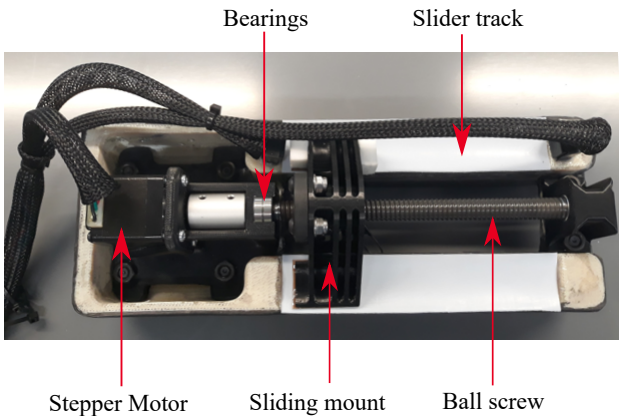

Fig. 3: Bottom view of the variable stiffness lever-arm.

Control™ stepper motor with 200 steps/rev. The linear actuator comprising the ball screw and the stepper motor has a travel of 0.085 m, allowing the lever-arm to vary from 0.17 m to 0.25 m, with 8500 discrete positions. Assuming small angle variation between the spring and the slider track across all slider positions, the torsional stiffness about the ankle joint is the product of the spring force F and the effective lever-arm length at any given slider position L. The spring force F is given by

$$F = k_{\text{s}} x \tag{1}$$

where x is the displacement of the spring's length, which scales with the effective length of the lever-arm L, and k_{s} is the stiffness constant of the spring in N/m. The calculation for the system's torsional stiffness simplifies to [18]

$$k_{\text{exo}} = k_{\text{s}} L^2, \tag{2}$$

where k_{exo} is the torsional stiffness of the exoskeleton about the ankle joint in Nm/rad. Thus, changing the lever-arm length from 0.17-0.25 m modifies the stiffness from 1-2.25 times the minimum torsional stiffness. For instance, we used a spring of 5.8 kN/m to implement a torsional stiffness range of 169-362 Nm/rad. This spring stiffness was chosen such that the optimum torsional stiffness as found in [3] lies in the above range. The total mass of the exoskeleton frame including the variable stiffness lever was 1323 g.

Remark 1: *The stepper motor in our variable stiffness mechanism varies only the torsional joint stiffness and does not provide power to the joint, which allows us to select a small low-power motor. For designs that power the ankle joint directly, we recommend the reader to review the state-of-art variable stiffness actuators such as the MACCEPA [19], [20]. Note that powering the ankle joint directly requires heavier actuators than our proposed mechanism.*

C. Embedded Systems and Sensing

All sensing, data recording, ESC implementation (detailed in Section II-D) and motor controls were performed on-board using an Arduino Mega 2560 microcontroller. The muscular effort of the soleus and tibialis anterior muscles were measured by two Myoware™ EMG sensors (AT-04-001). The Myoware sensor provided on-board amplification, rectification, and integration, which was utilized to reduce processing demand on the system's controller. To protect the raw EMG signal from interference, all wires carrying unamplified EMG signals were double shielded. The stepper motors were powered by two 2300 mAh 12V nickel metal hydride batteries connected in series to provide 24 V with a total battery capacity of 55.2 W-h. All the components above were secured to a padded belt, which was worn at the user's waist, as shown in Fig. 1a. The total weight of the belt containing all of the components and the batteries was 1750 g. Data and power cables were run laterally down the user's leg, connecting the controller to the sensors and motors.

D. Discrete ESC for Stepper Motors

ESC is a *model-free* adaptive control method that finds an optimum set-point in order to minimize/maximize an objective function, whose analytical expression might be unknown [9], [21]–[23]. Fig. 4 shows a block diagram of a discrete-time ESC with a human-in-the-loop. We modified the structure of conventional discrete-time ESC [24] by observing that the stepper motor dynamics already have an integrator [25]. In particular, we moved the ESC integrator in the conventional ESC structure ahead of the summer block. In this modified structure, the ESC integration is performed by the motor dynamics itself.

In order to understand the benefit of this ESC structure for implementation with a stepper motor, we first briefly explain the stepper motor operation. A stepper motor runs on a pulsed current, where each pulse turns the motor a fraction of the full rotation. It does not have any closed-loop encoder feedback for position control. Instead it accepts a *change* in the motor location as an input command instead of the *final* motor location. The purpose of modifying the structure of conventional discrete-time ESC in [24] was specifically done to satisfy this requirement of stepper motors.

Remark 2: *The modified structure of ESC algorithm is a discretized version of ESC presented in [26]–[28] and is more suitable for implementation with stepper motor than the conventional ESC structure for the reasons stated above. The conventional ESC structure would have commanded the final motor location, whereas our modified structure commands a change in the motor location.*

The working of the discrete-time ESC can be explained as follows. The ESC algorithm adds a small periodic perturbation signal $d_1(k) = -a\omega \sin(\omega k)$, known as the dither signal, to the commanded change in the motor location $\Delta\theta(k)$. Assume that the stepper motor dynamics is modeled as a cascade connection of a zero-order hold and a continuous-time integrator. The zero-order hold circuit holds the sample $\Delta\theta(k)+d_1(k)$ constant for one sampling interval ΔT. Denoting t_k as the sampling time, the expression for $\dot{\theta}(t_k)$ can be written as $\dot{\theta}(t_k) \approx \Delta\theta(k)/\Delta T - a\omega \sin(\omega t_k)$. The integrator dynamics of the stepper motor then outputs $\theta(t_k)+a\cos(\omega t_k)$, where $\theta(t_k)$ is the position of the stepper motor at time t_k. The objective function $J(\cdot)$ (e.g., muscular effort) measured at this motor position is sampled to give $J(\theta(k) + a\cos(\omega k))$. The Taylor series approximation of

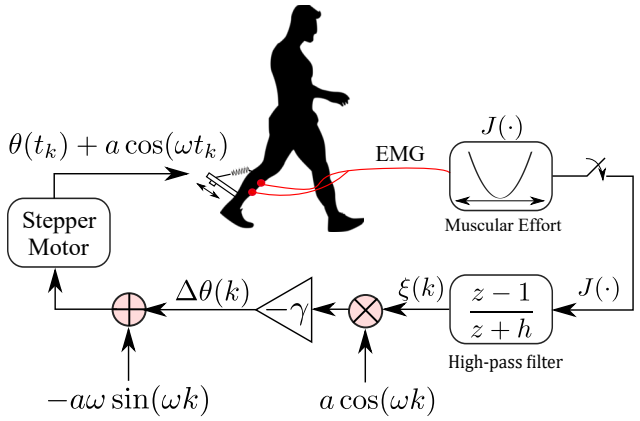

Fig. 4: Block diagram of a perturbation-based discrete ESC with a human-in-the-loop. The ESC commands a change in the stepper motor location $\Delta\theta(k)$, which moves the spring set-point in the lever-arm. With the new effective lever-arm length, the user walks and the EMG readings are measured to quantify the objective function $J(\cdot)$.

$J(\theta(k)+a\cos(\omega k))$ can be written as

$$J(\cdot)\approx J(\theta(k))+J'(\theta(k))a\cos(\omega k)+\frac{J''(\theta(k))}{2}a^2\cos^2(\omega k)$$
$$=J(\theta(k))+J'(\theta(k))a\cos(\omega k)+\frac{a^2J''(\theta(k))}{4}(1+\cos 2(\omega k)), \quad (3)$$

where J', J'' are the first and the second derivatives of $J(\cdot)$ with respect to θ. The objective function measurements in (3) are passed through a high-pass filter (HPF), which removes the DC components $J(\theta(k))$ and $a^2J''(\theta(k))/4$ to give

$$\xi(k) = J'(\theta(k))a\cos(\omega k) + \frac{a^2J''(\theta(k))}{4}\cos(2\omega k). \quad (4)$$

The output of the HPF $\xi(k)$ is then multiplied by another dither signal $a\cos(\omega k)$ and scaled by a gain $-\gamma$ to generate

$$\Delta\theta(k)=-\gamma\left[J'(\cdot)a\cos(\omega k)+\frac{a^2J''(\cdot)}{4}\cos(2\omega k)\right]a\cos(\omega k)$$
$$=-\gamma\left[\frac{a^2J'(\cdot)}{2}[1+\cos(2\omega k)]+\frac{a^3J''(\cdot)}{4}\cos(2\omega k)\cos(\omega k)\right], \quad (5)$$

which indicates the amount that the motor should move in order to minimize the cost function. From (5), it can be seen that $\Delta\theta(k)$ consists of a DC component, which is proportional to $J'(\cdot)$, and contains other higher frequency terms. Following standard manipulations (see [24]), the update equations of discrete-time ESC can be written as

$$\xi(k) = -h\xi(k-1) + J(\theta(k)) - J(\theta(k-1)) \quad (6)$$
$$\Delta\theta(k) = -\gamma[\xi(k)a\cos(\omega k)] \quad (7)$$

where γ is the adaptation gain and $h \in (0,1)$ is the HPF cut-off frequency. The stability of the algorithm can be proved based on two-time scale averaging theory (see [24] for further details).

E. ESC Code Implementation

The code for the ESC controlled system runs in 3 nested loops: the ESC loop, the aggregation loop, and the gait detection loop. The gait detection loop is the innermost loop, whose primary function is to read all sensors and record data as well as detect each gait cycle using the 2 FSRs. In each iteration of this loop, the rectified EMG readings from both the tibialis anterior and soleus muscles were summed and then integrated over a gait cycle using a rectangular integration method with a step size of 0.033 seconds. Once a gait cycle is detected, the aggregation loop adds the area for the step that was just detected to an aggregated area value. This process continues until 3 gait cycles are detected. The aggregated area value, containing the total integrated EMG area for the previous 3 gait cycles, is then used as an objective function input to the ESC algorithm. We chose 3 gait cycles for computing the objective function to achieve a balance between the robustness and the convergence rate of ESC adaptation. A pseudo code for the ESC operational loop is available for download in the supplementary materials.

Remark 3: *The integration that occurs in the gait detection loop converts the instantaneous EMG signals into a meaningful value that quantifies the total muscular effort of each step. The aggregation loop acts as a filter on the inherent noise of the biological signal by combining multiple steps.*

III. Experimental Setup and Protocol

A. Experimental Setup

The experiment protocol was approved by the Institutional Review Board (IRB) at the University of Texas at Dallas. Experiments were conducted with a healthy subject wearing the ankle exoskeleton while walking on a treadmill. Two EMG sensors were placed on the soleus and the tibialis anterior muscles after skin preparation to measure the muscular effort at 30 Hz. In order to normalize the EMG readings, a maximum voluntary contraction (MVC) experiment was first conducted, in which the user was instructed to flex each muscle as hard as possible. The skin preparation, sensor placement, and the MVC experimental procedures followed the guidelines suggested in [29]. This MVC experiment was conducted just once prior to the start of sweep and ESC experiments (see Section IV-A, IV-B).

Prior to testing, the subject was fitted with an ankle exoskeleton and given a chance to acclimate to it, while the electrical control was disabled. During the acclimation period, the torsional stiffness of the exoskeleton was fixed at a median value of 194 Nm/rad. After acclimation, the subject was instructed to walk on the treadmill at 1.0 m/s and 1.5 m/s for up to 5 minutes for baseline walking experiments (see Section IV-A) and up to 15 minutes for ESC walking experiments (see Section IV-B), whose protocols are discussed next. All experiments were done on level ground on the same day, and the user was given sufficient rest in between the experiments to avoid fatigue.

B. Experiment Protocol for Baseline Walking Experiments

Following acclimation, the user was asked to walk on a treadmill at 1 m/s until 30 gait cycles of data had been collected. At that point the slider would advance to the next equally spaced slider position and another 30 gait cycles of

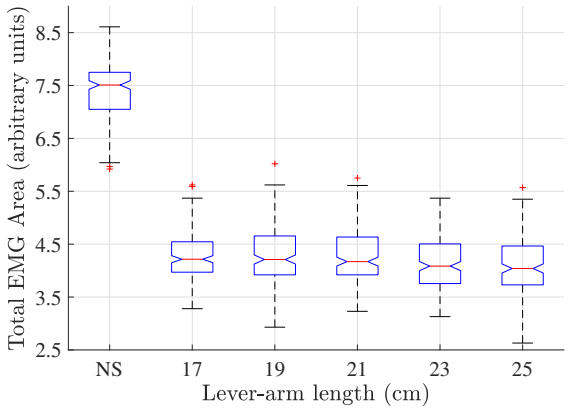

(a) Baseline walking experiment result at slow walking speed (1 m/s), indicating the minimum median muscle effort at lever-arm length L=25 cm.

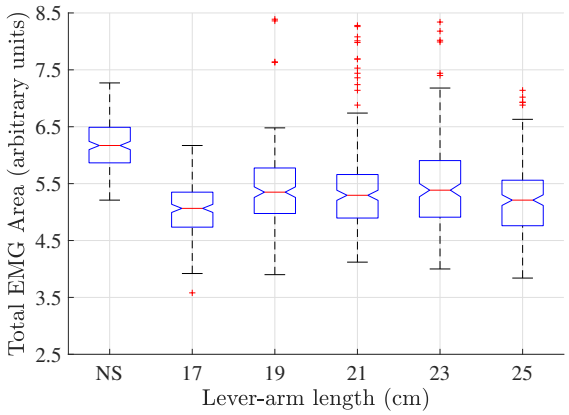

(b) Baseline walking experiment result at fast walking speed (1.5 m/s), indicating the minimum median muscle effort at lever-arm length L=17 cm.

Fig. 5: Box plot of baseline and no spring (NS) tests at different walking speeds. The x-axis indicates the lever-arm length L, with L=17 cm and L=25 cm being closest and farthest from the ankle joint, respectively. It can be seen that the EMG readings are higher at fast walking speed as compared to slow walking speed. It can also be seen that each walking speed has a different optimum lever-arm length that minimizes the median muscular effort, thus necessitating the need for real-time adaptation with changes in walking speed.

data were recorded. This process continued until 5 equally spaced positions had been tested from one end of the lever-arm to the other end. In this manner, the user's muscular effort response to the full range of torsional stiffness was tested. This process lasted for approximately 5 minutes, with a total of 150 gait cycles being recorded. Steps taken during slider adjustment were removed from the data set and were not included in the above mentioned step count. Due to the variation in the gait patterns, the muscular effort during each step was different. Therefore, we conducted 6 baseline walking trials, giving 180 steps of data for each slider location. Following this, the same protocol was repeated for fast walking speed (1.5 m/s).

C. Experiment Protocol for ESC Walking Experiments

After baseline testing, the user walked on a treadmill for 15 minutes per experiment. Two versions of this experiment were performed —slow-fast-slow (SFS) and fast-slow-fast (FSF). For SFS testing, the user was instructed to walk at 1 m/s for 5 minutes. At the 5 minute point, the treadmill speed was increased to 1.5 m/s, which was maintained for another 5 minutes. At the 10 minute point, the treadmill speed was reduced back to 1 m/s and held for another 5 minutes. Similarly, the FSF case started and ended at 1.5 m/s, with the same time intervals for the three speed conditions.

IV. Experimental Testing Results

A. Baseline Walking Experiments

There were two main goals for performing baseline walking trials. First, we wanted to demonstrate that a change in the slider location affects the muscular effort during walking. Second, as the optimum slider location for different walking speeds was not known a priori, we wanted to experimentally determine the optimum slider location for this subject at different walking speeds. This information helps us validate the real-time ESC adaptation results across different walking speeds in Section IV-B.

In order to show the effect of slider location on the muscular effort, we grouped the EMG readings from all experiments by slider locations. This resulted in 180 sample data points per slider location (i.e., 30 samples/test $\times$ 6 tests). A control test was also performed with no spring (NS). Figs. 5a, 5b show box plots obtained from 6 baseline and NS tests for slow and fast walking speeds, respectively. Two important observations can be made from this result: (i) By comparing Figs. 5a, 5b it can be noted that the optimum slider location for slow walking speed (L=25 cm at 1 m/s) is higher than that for fast walking speed (L=17 cm at 1.5 m/s); and (ii) Due to the variations in the gait pattern, there are multiple local optimums. Note that due to the complex landscape of the objective function, our ESC algorithm would only be able to tune the system to a local minimum.

Next, we ran Lilliefors test for normality and found that the EMG data at each slider location was not normally distributed. In such a case, a non-parametric test, such as Friedman, Kolmogorov–Smirnov, Wilcoxon signed-rank, should be performed [30]. We first conducted a Friedman's test to check the validity of the null hypothesis that all samples taken at different slider locations come from the same distribution. The Friedman's test, performed in MATLAB, returned a $p-$value of 7.4×10^{-9} for slow and 2.6×10^{-14} for fast walking speeds, which is much less than the significant threshold of 0.05. This implies that we can reject the null hypothesis and conclude that a change in slider location makes a difference in the muscular effort for this subject. Next, we conducted Wilcoxon signed-rank statistical tests for EMG data collected at each pair of slider locations. We chose Wilcoxon signed-rank over other non-parametric tests because it performs *paired* hypothesis testing and assumes *dependent* data samples. In our case, a paired hypothesis testing is suitable because the same muscle readings are recorded multiple times at different slider locations. Also, since the EMG readings for this subject come from the same muscles, the EMG data at different slider locations are

TABLE I: Pairwise Wilcoxon signed-rank test results between different slider locations L at slow and fast speed.

(a) p-values from Wilcoxon signed-rank test at slow speed.

L (cm)	Lever-arm length L (cm)				
	17	19	21	23	25
17	1.0000	0.6011	0.3118	0.0028*	0.0001*
19	0.6011	1.0000	0.7135	0.0021*	0.0000*
21	0.3118	0.7135	1.0000	0.0000*	0.0000*
23	0.0028*	0.0021*	0.0000*	1.0000	0.2131
25	0.0001*	0.0000*	0.0000*	0.2131	1.0000

(b) p-values from Wilcoxon signed-rank test at fast speed.

L (cm)	Lever-arm length L (cm)				
	17	19	21	23	25
17	1.0000	0.0000*	0.0000*	0.0000*	0.0002*
19	0.0000*	1.0000	0.0001*	0.0258	0.0000*
21	0.0000*	0.0001*	1.0000	0.3870	0.0008*
23	0.0000*	0.0258	0.3870	1.0000	0.0000*
25	0.0002*	0.0000*	0.0008*	0.0000*	1.0000

dependent. We formulated a null hypothesis that the median difference between the EMG data at different slider locations (excluding NS) is zero. The p values for all combinations of slider locations at different walking speeds are tabulated in Table I. An asterisk at the end of p-value indicates statistical significance between the pair of slider locations. Tables Ia and Ib show that the effect of the slider location on the muscular effort varies across walking speed.

To avoid false reporting of significant differences in multiple pairwise comparisons, we use the Bonferroni-corrected threshold value of 0.005. For slow walking speed, it can be seen from Table Ia that there are 2 groups of slider locations that result in statistically different EMG data for this subject, based on a threshold of $p = 0.005$. One group comprises slider locations L=17, 19 and, 21 cm, and the other group comprises slider locations L=23 and 25 cm. Similarly, for fast walking speed, we see from Table Ib that the EMG data at all slider locations (except between L=19 and 23 cm and L=21 and 23 cm) are statistically different for this subject.

Remark 4: *Figs. 5a, 5b show that the EMG readings are higher for no spring as compared to with spring for both slow and fast walking speeds, thus clearly indicating the benefit of using the spring in the device.*

B. ESC Walking Experiments

Fig. 6 shows the ESC adaptation results for the two different experimental scenarios discussed in Section III. The ESC parameters selected were $a = 2, \gamma = -10, \omega = 0.55$Hz, $h = 0.5$Hz, according to the guidelines mentioned in [9]. Because the walking speed was changed based on time (after every 5 minutes), the fast walking regime has more ESC iterations as compared to the slow walking. In the slow regimes (first and third regime of Fig. 6a and second regime of Fig. 6b), we see that the lever-arm length increases and eventually approaches a steady-state, which in turn reduces the muscle effort. This is exactly in accordance with the baseline walking experimental results in Section IV-A. Next,

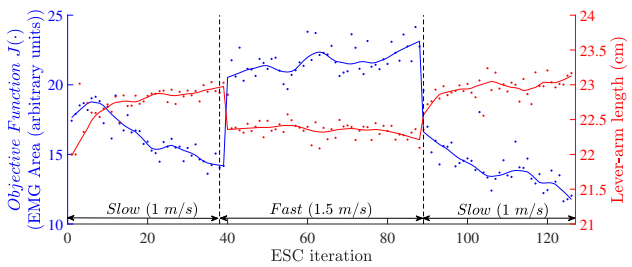

(a) Slow-Fast-Slow ESC experiment

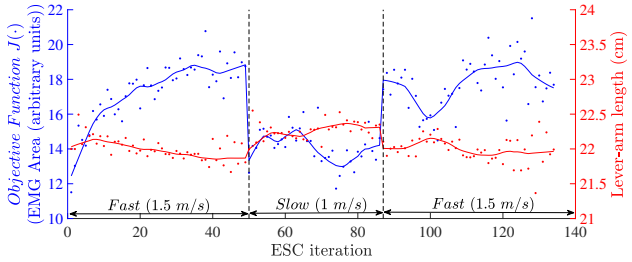

(b) Fast-Slow-Fast ESC experiment

Fig. 6: Real-time ESC adaptation of lever-arm length (torsional stiffness) across different walking speeds. The blue dots are the accumulated EMG area for 3 gait cycles (one ESC iteration), and the red dots are the lever-arm lengths at a particular ESC iteration. The solid blue and red lines are fitted by smoothing the data using locally weighted linear regression. The vertical black dashed lines indicate the ESC iteration at which the walking speed was changed. It can be seen that ESC quickly adapts the lever-arm position in response to change in muscular effort at walking speed transitions.

at the speed transitions, we see a sudden change in the muscle effort followed by a rapid ESC adaptation of the lever-arm length in the direction we expect. At fast speed regimes (second regime of Fig. 6a and first and third regime of Fig. 6b), we see the lever-arm length decreasing as we expect. However, we do not see a dramatic reduction in the muscle effort, which we explore more in Section V.

Fig. 7 shows the average EMG readings for tibialis anterior and soleus muscles at slow walking speed. The blue and red lines represent the average of EMG readings across gait cycles during the first and the last minute of slow speed walking, respectively. It can be noted that the average EMG readings for both of the tibialis anterior and soleus muscles decreased significantly after ESC adaptation. In particular, the average RMS EMG readings of tibialis anterior and soleus muscles decreased by 26.48% and 7.42%, respectively. From (2), we see that changing the lever-arm length from L=23 cm to L=22 cm decreases the torsional stiffness k_{exo} by 9.3%. A supplemental video of the experiment is available for download.

V. Discussion

A. Walking Experiment Results

Two important observations can be made from the ESC adaptation results in Fig. 6. First, ESC rapidly changes the effective lever-arm length in response to changes in the muscular effort across walking speeds. Second, the tuned

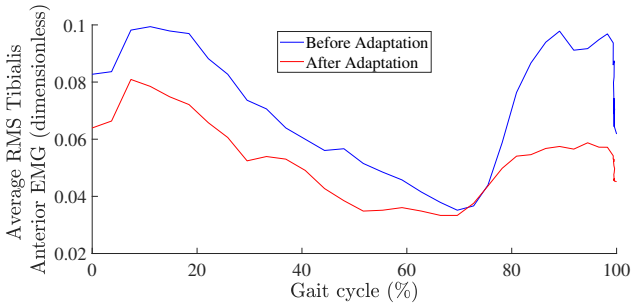

(a) Average tibialis anterior EMG readings

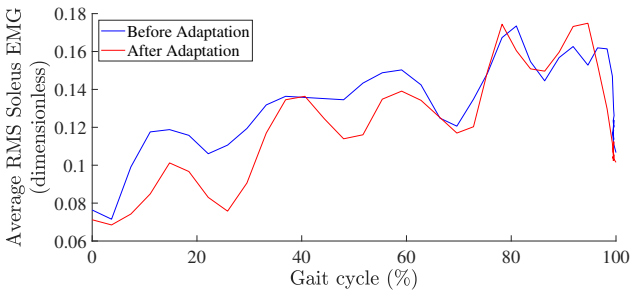

(b) Average soleus EMG readings

Fig. 7: Average EMG readings for tibialis anterior and soleus muscles before and after ESC adaptation at slow walking speed. The average RMS value of tibialis anterior and soleus muscle activity decreased by 26.48% and 7.42%, respectively.

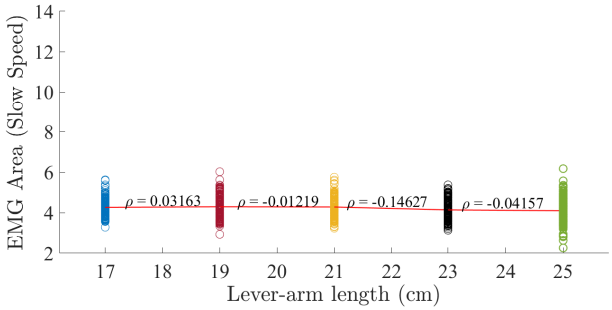

(a) Scatter plot of EMG area at slow walking speed

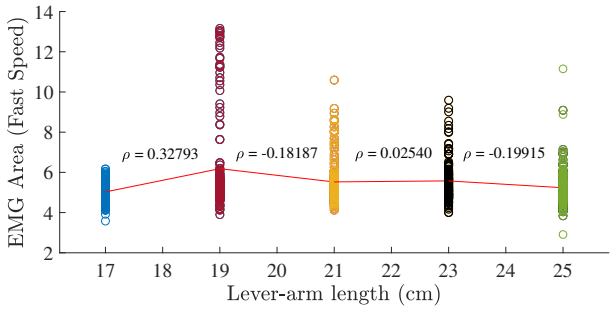

(b) Scatter plot of EMG area at fast walking speed

Fig. 8: Scatter plot of EMG area at different slider locations for different walking speeds and pairwise correlation coefficients ρ. The red line (with slope=ρ) represents a least square line fit to the EMG data between two consecutive lever-arm lengths.

TABLE II: Variance in EMG readings at different slider locations in slow and fast walking baseline experiments.

Walking Speed	Lever-arm length (cm)				
	17	19	21	23	25
Slow (1 m/s)	0.3402	0.4207	0.3323	0.4230	0.5574
Fast (1.5 m/s)	1.1436	5.9647	1.3239	4.6035	0.8425

lever-arm position decreases the steady-state muscular effort in the slow walking speed regimes.

However, in the fast speed regimes, we do not see a net reduction in the steady-state muscular effort in response to the change in the slider location. To explain this observation, we computed pairwise correlation coefficients between EMG readings at successive slider locations. Fig. 8 shows a scatter plot of EMG area at different slider locations for slow and fast walking speeds and pairwise correlation coefficients ρ between successive lever-arm positions. It can be noted from Fig. 8a that in slow speed, $\rho < 0$ for all lever-arm positions between 19-25 cm. This indicates that the lever-arm length and the EMG area are *uniformly* negatively correlated. However, from Fig. 8b, it can be seen that at fast speed, the sign of the correlation coefficient ρ keeps alternating, i.e., between slider location 17-19 cm, $\rho > 0$, and between 19-21 cm, $\rho < 0$, and so on. This implies that for certain slider locations, the EMG area and the lever-arm length are positively correlated while at other locations, they are negatively correlated. Also, it can be observed from Fig. 8 that the variance of EMG readings is much higher for fast speed as compared to the slow speed walking. Table II shows the variance in the EMG readings at different slider locations for slow and fast walking speeds. The alternating signs of the correlation coefficient between two successive lever-arm lengths at fast walking speeds indicates the presence of multiple optimums in the objective function. Due to high variance in the EMG data at fast speeds, we might have to run the walking experiments for a longer duration to see the expected decrease in the muscular effort.

Although we do not see a net reduction in the steady-state muscular effort in the fast speed regimes, we can observe from Figs. 6a and 6b that the ESC tunes the stiffness of the device at fast walking speeds. Notice that the red graph in the slow walking regime (see Fig. 6a) converges to $L = 23$ cm and in the fast walking regime (see Fig. 6b) to $L = 22$ cm. This implies that the local optima for slow and fast walking speeds are $L = 23$ cm and $L = 22$ cm, respectively. Furthermore, from Fig. 6a, it can be seen that as the walking speed changes from slow to fast, ESC gradually tunes the lever-arm length in the appropriate direction (towards $L = 22$ cm, i.e., optimum for fast walking) in the fast speed regime. Now, if the user would have walked with the lever-arm length fixed to $L = 23$ cm at fast walking speed, it would have led to an increase in the muscular effort. This can be observed from Fig. 8b, where the correlation coefficient is positive between slider locations 21 and 23 cm.

B. Limitations

Our experimental results were based on data collected from a single able-bodied subject. Our study to this point is based on six baseline walking experiments to understand

the effect of walking speed on the optimum slider location. We did not investigate the impact of our exoskeleton on the normative kinematics of the able-bodied subject. Further study should test more subjects with motion capture to analyze biomechanical implications such as the effect on gait kinematics and kinetics.

Our research goal is to establish the efficacy of real-time optimization on quasi-passive exoskeletons. Therefore, our preliminary design, which has a long lever-arm that protudes from the back of the shank, might not be optimal for real-world use. Further development of the system by redesigning the variable stiffness adjustment system could make the device lighter and more compact, while maintaining the range of adjustment. A reduction in the lever-arm would also allow a smaller but stiffer spring to be used to further reduce weight, allowing for even greater improvements to walking efficiency. A novel under-shoe clutching design presented in [4] could be implemented to reduce muscle activation further by engaging the variable stiffness mechanism at specific times within the gait cycle, as shown in [3].

VI. CONCLUSIONS

We developed a quasi-passive exoskeleton that combines the adaptability of active exoskeletons with the light-weight and autonomy of passive exoskeletons. The ESC we developed alongside this exoskeleton is capable of continuous adaptation and autonomous operation. By combining highly efficient stiffness adjustment and a computationally inexpensive controller, our walking experiments demonstrated that ESC was able to automatically tune the torsional stiffness of the ankle exoskeleton based on bio-feedback received from the EMG sensor across different walking speeds. In future, a time-invariant framework of ESC [31] could be used to improve the performance of the algorithm. To facilitate a comprehensive study, future work should include indirect calorimetry to quantify reduction of metabolic cost.

ACKNOWLEDGMENT

The authors thank the UTD senior design team for building a preliminary version of the quasi-passive ankle exoskeleton.

REFERENCES

[1] D. J. Farris, B. D. Robertson, and G. S. Sawicki, "Elastic ankle exoskeletons reduce soleus muscle force but not work in human hopping," *J. Appl. Physiol.*, vol. 115, no. 5, pp. 579–585, 2013.

[2] D. J. Farris and G. S. Sawicki, "Linking the mechanics and energetics of hopping with elastic ankle exoskeletons," *Journal of Applied Physiology*, vol. 113, no. 12, pp. 1862–1872, 2012.

[3] S. H. Collins, M. B. Wiggin, and G. S. Sawicki, "Reducing the energy cost of human walking using an unpowered exoskeleton," *Nature*, vol. 522, no. 7555, p. 212, 2015.

[4] M. B. Yandell, J. R. Tacca, and K. E. Zelik, "Design of a low profile, unpowered ankle exoskeleton that fits under clothes: Overcoming practical barriers to widespread societal adoption," *IEEE Trans. Neural Syst. Rehabil. Eng.*, vol. 27, no. 4, pp. 712–723, 2019.

[5] M. H. Schwartz, A. Rozumalski, and J. P. Trost, "The effect of walking speed on the gait of typically developing children," *Journal of biomechanics*, vol. 41, no. 8, pp. 1639–1650, 2008.

[6] J. Zhang *et al.*, "Human-in-the-loop optimization of exoskeleton assistance during walking," *Science*, vol. 356, no. 6344, pp. 1280–1284, 2017.

[7] S. Lee *et al.*, "Autonomous multi-joint soft exosuit with augmentation-power-based control parameter tuning reduces energy cost of loaded walking," *J Neuroeng Rehabil*, vol. 15, no. 1, p. 66, 2018.

[8] J. R. Koller, D. H. Gates, D. P. Ferris, and C. D. Remy, "Body-in-the-Loop Optimization of Assistive Robotic Devices: A Validation Study," in *Proceedings of Robotics: Science and Systems*, AnnArbor, Michigan, June 2016.

[9] S. Kumar, A. Mohammadi, D. Quintero, S. Rezazadeh, N. Gans, and R. D. Gregg, "Extremum seeking control for model-free auto-tuning of powered prosthetic legs," *IEEE Trans. Control Syst. Technol.*, pp. 1–16, 2019.

[10] R. W. Jackson and S. H. Collins, "Heuristic-based ankle exoskeleton control for co-adaptive assistance of human locomotion," *IEEE Trans. Neural Syst. Rehabil. Eng.*, vol. 27, no. 10, pp. 2059–2069, 2019.

[11] K. E. Gordon and D. P. Ferris, "Learning to walk with a robotic ankle exoskeleton," *J Biomech*, vol. 40, no. 12, pp. 2636–2644, 2007.

[12] G. S. Sawicki and D. P. Ferris, "Mechanics and energetics of level walking with powered ankle exoskeletons," *Journal of Experimental Biology*, vol. 211, no. 9, pp. 1402–1413, 2008.

[13] J. R. Koller, D. A. Jacobs, D. P. Ferris, and C. D. Remy, "Learning to walk with an adaptive gain proportional myoelectric controller for a robotic ankle exoskeleton," *Journal of neuroengineering and rehabilitation*, vol. 12, no. 1, p. 97, 2015.

[14] C. J. Walsh, K. Endo, and H. Herr, "A quasi-passive leg exoskeleton for load-carrying augmentation," *International Journal of Humanoid Robotics*, vol. 04, no. 03, pp. 487–506, 2007.

[15] C. J. Walsh, D. Paluska, K. Pasch, W. Grand, A. Valiente, and H. Herr, "Development of a lightweight, underactuated exoskeleton for load-carrying augmentation," in *IEEE International Conference on Robotics and Automation.*, May 2006, pp. 3485–3491.

[16] D. P. Allen, E. Bolívar, S. Farmer, W. Voit, and R. D. Gregg, "Mechanical Simplification of Variable-Stiffness Actuators Using Dielectric Elastomer Transducers," *Actuators*, vol. 8, no. 2, p. 44, may 2019.

[17] M. S. Stanković and D. M. Stipanović, "Extremum seeking under stochastic noise and applications to mobile sensors," *Automatica*, vol. 46, no. 8, pp. 1243–1251, 2010.

[18] L. C. Visser, R. Carloni, and S. Stramigioli, "Energy-efficient variable stiffness actuators," *IEEE Trans. Robot.*, vol. 27, no. 5, pp. 865–875, 2011.

[19] B. Vanderborght *et al.*, "MACCEPA 2.0: compliant actuator used for energy efficient hopping robot Chobino1D," *Auton. Robots*, vol. 31, no. 1, pp. 55–65, jul 2011.

[20] ——, "Variable impedance actuators: A review," *Rob. Auton. Syst.*, vol. 61, no. 12, pp. 1601–1614, dec 2013.

[21] M. Krstić and H.-H. Wang, "Stability of extremum seeking feedback for general nonlinear dynamic systems," *Automatica*, vol. 36, no. 4, pp. 595–601, 2000.

[22] K. B. Ariyur and M. Krstic, *Real-time optimization by extremum-seeking control*. John Wiley & Sons, 2003.

[23] S. Kumar, A. Mohammadi, N. Gans, and R. D. Gregg, "Automatic tuning of virtual constraint-based control algorithms for powered knee-ankle prostheses," in *2017 IEEE Conf. on Control Tech. and App.*, pp. 812–818.

[24] Joon-Young Choi, M. Krstic, K. B. Ariyur, and J. S. Lee, "Extremum seeking control for discrete-time systems," *IEEE Transactions on Automatic Control*, vol. 47, no. 2, pp. 318–323, Feb 2002.

[25] A. Morar, "Stepper motor model for dynamic simulation," *IEEE Transc. Automatic Control*, vol. 44, no. 2, pp. 117–122, 2003.

[26] C. Zhang, A. Siranosian, and M. Krstić, "Extremum seeking for moderately unstable systems and for autonomous vehicle target tracking without position measurements," *Automatica*, vol. 43, no. 10, pp. 1832–1839, 2007.

[27] M. S. Stanković, H.-B. Dürr, and K. H. Johansson, "A lie bracket approximation for extremum seeking vehicles," *IFAC Proceedings Volumes*, vol. 44, no. 1, pp. 11 393 – 11 398, 2011.

[28] H.-B. Dürr, M. S. Stanković, C. Ebenbauer, and K. H. Johansson, "Lie bracket approximation of extremum seeking systems," *Automatica*, vol. 49, no. 6, pp. 1538–1552, 2013.

[29] H. J. Hermens *et al.*, "European recommendations for surface electromyography," *Roessingh research and development*, vol. 8, no. 2, pp. 13–54, 1999.

[30] B. Rosner, *Fundamentals of Biostatistics*. Cengage Learning, 2015.

[31] S. Kumar, A. Mohammadi, R. D. Gregg, and N. Gans, "Limit cycle minimization by time-invariant extremum seeking control," in *American Control Conference*, 2019, pp. 2359–2365.